Research Square

Preprints are preliminary reports that have not undergone peer review.
They should not be considered conclusive, used to inform clinical practice,
or referenced by the media as validated information.

Functional CeO_x nanoglues for efficient and robust atomically dispersed catalysts

Jingyue Liu (jingyueliu@msn.com)
Arizona State University
Xu Li
Arizona State University
Xavier Isidro Pereira Hernandez
Washington State University https://orcid.org/0000-0002-7020-0011
Chia-Yu Fang
University of California-Davis
Yizhen Chen
University of California
Jie Zeng
University of Science and Technology of China https://orcid.org/0000-0002-8812-0298
Yong Wang
Washington State University
Bruce Gates
University of California, Davis https://orcid.org/0000-0003-0274-4882

Physical Sciences - Article

Keywords: single-atom catalysts (SACs), nanoglues, catalytic transformations

Posted Date: June 24th, 2021

DOI: https://doi.org/10.21203/rs.3.rs-604924/v1

License: This work is licensed under a Creative Commons Attribution 4.0 International License.
Read Full License

Version of Record: A version of this preprint was published at Nature on October 26th, 2022. See the published version at https://doi.org/10.1038/s41586-022-05251-6.

Abstract

Single-atom catalysts (SACs) exhibit unique catalytic property and maximum atom efficiency of rare, expensive metals. A critical barrier to applications of SACs is sintering of active metal atoms under operating conditions. Anchoring metal atoms onto oxide supports via strong metal-support bonds may alleviate sintering. Such an approach, however, usually comes at a cost: stabilization results from passivation of metal sites by excessive oxygen ligation—too many open coordination sites taken up by the support, too few left for catalytic action. Furthermore, when such stabilized metal atoms are activated by reduction at elevated temperatures they become unlinked and so move and sinter, leading to loss of catalytic function. We report a new strategy, confining atomically dispersed metal atoms onto functional oxide nanoclusters (denoted as nanoglues) that are isolated and immobilized on a robust, high-surface-area support—so that metal atoms do not sinter under conditions of catalyst activation and/or operation. High-number-density, ultra-small and defective CeOx nanoclusters were grafted onto high-surface-area SiO2 as nanoglues to host atomically dispersed Pt. The Pt atoms remained on the CeOx nanoglue islands under both O2 and H2 environment at high temperatures. Activation of CeOx supported Pt atoms increased the turnover frequency for CO oxidation by 150 times. The exceptional stability under reductive conditions is attributed to the much stronger affinity of Pt atoms for CeOx than for SiO2—the Pt atoms can move but they are confined to their respective nanoglue islands, preventing formation of larger Pt particles. The strategy of using functional nanoglues to confine atomically dispersed metal atoms and simultaneously enhance catalytic performance of localized metal atoms is general and takes SACs one major step closer to practical applications as robust catalysts for a wide range of catalytic transformations

Main Text

The design strategy integrates three components into the final catalyst: 1) a robust, high-surface-area support (e.g., SiO_2, Al_2O_3, etc.), 2) nanoscale functional metal oxides (e.g., CeO_x, TiO_x, FeO_x, etc.) anchored stably onto the robust support as isolated nanoglue islands, and 3) single metal atoms (M_1) selectively localized to only the nanoglue islands. The nanoglue selection criteria include a) its *stability in dispersed form on the support* surface due to strong bonding, b) a much *stronger affinity for the active metal atoms than the support,* and c) *interactions with the active metal that enhance activity and/or selectivity* for the desired catalytic reactions. The selected nanoglue not only behaves as a “double-sided tape” but also contributes to the desired functions for the targeted catalytic reaction.

We selected SiO_2, an irreducible, inexpensive support widely used in processing industries, to demonstrate our strategy because of its high-surface-area, structural stability, and availability in various forms[14]. Because metal atoms anchor onto reducible metal oxides (e.g., CeO_2, TiO_2, Fe_2O_3, Co_3O_4, etc.) at defect sites and/or via formation of strong M_1-O_x bonds[8,15-18], and ceria has unique redox and oxygen-storage properties[19,20], we choose CeO_x nanoclusters as prototype nanoglues to localize Pt atoms for CO oxidation reaction. The critical aspect of this new design strategy is to produce ultra-small, isolated CeO_x

nanoclusters uniformly distributed on high-surface-area SiO_2 support via a scalable/practical synthesis process.

Uniform CeO_x nanocluster islands were synthesized by strong electrostatic adsorption (SEA) of charged species from aqueous solution[21], as schematically illustrated in Fig. 1. The point of zero charge (PZC) of the high-surface-area SiO_2 (278 m^2/g) is ~3.6 (ref.21), implying that its surface is negatively charged in an aqueous solution with pH > 4.0. Control of the solution OH^- concentration and adsorption time yielded soluble cationic $[Ce(OH)_x]^{y+}$ species that quickly adsorbed onto the SiO_2 surfaces, leading to (after a high-temperature calcination) formation of uniformly dispersed CeO_x nanoclusters. Short adsorption time (< 3 min) usually produces uniformly coated Ce species while extended adsorption time leads to formation of large CeO_2 particles (Extended Data Fig. 1a-b). High-angle annular dark-field scanning transmission electron microscope (HAADF-STEM) images showed uniform coating of the mesoporous SiO_2 support with Ce species as a result of the SEA process (Extended Data Fig. 1c-e). Subsequent calcination at 600° C produced individual crystalline CeO_x nanoclusters stably anchored onto SiO_2 surfaces (Fig. 2a and Extended Data Fig. 1f-g). The CeO_x loading was 12 wt%, determined by inductively coupled plasma mass spectrometry (ICP-MS), and the average CeO_x nanocluster dimensions were 1.8 nm × 2.1 nm (Extended Data Fig. 1h-i), with ellipsoid shapes. Atomic-resolution HAADF-STEM images (Fig. 2b) show that all the as-synthesized CeO_x nanocluster are well crystallized and some show visible surface steps.

Powder X-ray diffraction (XRD) patterns of the as-synthesized CeO_x/SiO_2 show broad diffraction peaks that represent a cubic fluorite structure (Fig. 2c). In comparison, the two control samples (12 wt% CeO_2 nanoparticles (NPs) on SiO_2, denoted as CeO_2 NPs/SiO_2, and pure CeO_2 powders, made by an impregnation or precipitation method, as stated in Fig. 2c and Extended Data Fig. 2a) yielded strong diffraction peaks, demonstrating large sizes of the as-prepared CeO_2 NPs. HAADF-STEM images show that the as-prepared CeO_2 NPs have a wide size distribution (Extended Data Fig. 2b-c, e-f). Raman spectra show a broadened and red-shifted active mode from 462 to 448 cm^{-1}, suggesting significant lattice distortion in the as-synthesized crystalline CeO_x nanoclusters (Extended Data Fig. 2g)[22]. The additional Raman band near 600 cm^{-1} indicates presence of oxygen vacancies[22]. Measurements of lattice distances of the CeO_x nanoclusters in numerous HAADF-STEM images showed an expansion of the CeO_2{111} plane distance from 3.1 Å (bulk CeO_2) to 3.3 Å in the CeO_x nanoclusters (Extended Data Fig. 2h), in agreement with the slight shift of the XRD peaks to lower angles (Fig. 2c).

X-ray photoelectron spectroscopy (XPS) data (Fig. 2d and Extended Data Fig. 2d) show 28.7 %, 10.9 % and 8.4% Ce^{3+} species in CeO_x/SiO_2, CeO_2 and CeO_2 NPs/SiO_2, respectively[12,23]. The significantly increased number of Ce^{3+} sites on the as-synthesized CeO_x nanoclusters suggests more anchor sites for metal atoms[8,15,24]. The fact that XPS probes surfaces of nanometers in depth[23] implies that the $Ce^{3+}/(Ce^{3+} + Ce^{4+})$ ratio (estimated from the XPS data) can be used to estimate the average composition

of the CeO_x nanoclusters since the heights of the as-synthesized CeO_x nanoclusters are less than 2 nm. The estimated composition of the as-synthesized CeO_x nanoclusters is $CeO_{1.86}$. Analyses of H_2 temperature-programmed reduction (H_2-TPR) showed that the reduction temperature of "bulk" oxygen from the $CeO_{1.86}$ nanoclusters took place at ~492 °C (290 °C lower than that of CeO_2 powder) (Extended Data Fig. 2i), suggesting that full reduction of the as-synthesized $CeO_{1.86}$ nanoclusters is much easier than that of CeO_2 NPs, providing a route to facile formation of oxygen species. The as-synthesized ultra-small, isolated $CeO_{1.86}$ nanoclusters are crystalline in nature, possess high-number density of surface defect sites, and provide labile oxygen species—well-suited to strong bonding of isolated Pt atoms.

Selective deposition of Pt atoms to the $CeO_{1.86}$ nanoglue clusters (Fig. 1)—but not the SiO_2 support—via a synthesis protocol was accomplished by the SEA process: opposite-charged species attract, and like-charged species repel. Because CeO_2 and SiO_2 possess PZCs (points of zero charge) of ~8.1 (ref.25) and 3.6, respectively, the sign of the surface charges of these two materials should be opposite when the solution pH is adjusted to between 4.0 and 6.0. After slowly titrating the $PtCl_6^{2-}$ precursor into the $CeO_{1.86}/SiO_2$ solution, the positively charged $CeO_{1.86}$ nanoclusters strongly adsorbed the $PtCl_6^{2-}$ complexes while the negatively charged SiO_2 surfaces strongly repelled these negatively charged species. The XPS measurements showed that after the preferential Pt deposition the amount of Ce^{3+} species in the $CeO_{1.86}/SiO_2$ was retained, and residual chloride was not detectable, removed by high-temperature calcination of the as-synthesized $Pt/CeO_{1.86}/SiO_2$ catalysts (Extended Data Fig. 3a-c). To selectively synthesize SACs, the Pt loading was controlled to be $\leq$ 0.4 wt% (with respect to the $CeO_{1.86}$ nanoclusters) since the average number density of Pt atoms on each $CeO_{1.86}$ nanocluster in the 0.4 wt% $Pt/CeO_{1.86}/SiO_2$ catalyst was estimated to be less than one (~0.6) Pt atom per $CeO_{1.86}$ nanocluster (Extended Data Fig. 3d-f). The ICP-MS measurements showed that ~99 % of the adsorbed Pt species were deposited onto the $CeO_{1.86}$ nanoglues while negligible amount of Pt was deposited onto the SiO_2 control sample via the same SEA process (Extended Data Fig. 3d). These results clearly and unambiguously demonstrated selective deposition of Pt atoms onto only the CeO_x nanoglues via the SEA process which is scalable and industrially practical.

The location identification of metal atoms with respect to the support surface structure is critical to understanding the catalytic properties of SACs. Even though Pt or Au atoms on well-crystallized CeO_2 NPs have been reliably observed in atomic-resolution HAADF-STEM images[26], Pt atoms on ultra-small CeO_X nanoclusters could not be unambiguously identified (Extended Data Fig. 4a-c and Methods). After intensive investigations of HAADF-STEM imaging of $CeO_{1.86}/SiO_2$ supported Pt atoms/clusters, we concluded that Pt clusters with a size > 0.4 nm could be reliable detected by direct HAADF-STEM imaging (Extended Data Fig. 4d). Based on analyzing numerous atomic-resolution HAADF-STEM images of as-synthesized 0.4 wt% $Pt/CeO_{1.86}/SiO_2$ catalysts, we concluded that there were no Pt single atoms/clusters/particles on the SiO_2 surfaces (in agreement with the ICP-MS measurement of the control

sample) and all the Pt species were deposited only onto the $CeO_{1.86}$ nanoglue islands either in the form of single Pt atoms or Pt clusters with sizes < 0.4 nm.

The Pt L_{III}-edge X-ray absorption near-edge structure (XANES) and the Fourier transform radial distribution functions of the k^3-weighted extended X-ray absorption fine structure (EXAFS) spectra of the 0.4 wt% $Pt/CeO_{1.86}/SiO_2$ catalyst are displayed in Fig. 3a-b. The XANES spectra suggest that the oxidation state of the Pt species is very close to that of Pt in PtO_2, consistent with a previous report[27]. The EXAFS spectrum gives no evidence in the 0.4 wt% $Pt/CeO_{1.86}/SiO_2$ catalyst of a Pt–Pt shell, in contrast to what is commonly observed for Pt or PtO_2 NPs or clusters (Extended Data Fig. 5), bolstering the conclusion that the Pt species existed as single, isolated atoms. The coordination number of the Pt–O shell in the model was found to be 4.5 ± 0.5 with a bonding length of 1.97 ± 0.02 Å, consistent with the EXAFS analyses reported for site-isolated platinum anchored on ceria and iron oxide[1,27]. Diffuse-reflectance infrared Fourier-transform spectroscopy (DRIFTS) spectra on the 0.4 wt% $Pt/CeO_{1.86}/SiO_2$ catalyst show a well-defined peak at 2103 cm^{-1} (Fig. 3c), assignable to CO adsorbed on ionic single Pt atoms[8,18,28].

The behavior of Pt atoms in the $Pt/CeO_{1.86}/SiO_2$ SAC under various treatment conditions were extensively investigated by HAADF-STEM and CO DRIFTS methods. For comparison, Pt atoms supported on SiO_2 and CeO_2 were synthesized and evaluated as control catalysts. Under either a reducing or oxidizing environment at temperatures >300 °C, Pt atoms sintered significantly on the SiO_2 support (Extended Data Fig. 6), demonstrating extremely weak interactions between Pt atoms and the SiO_2 support[29]. On the other hand, CeO_2-supported Pt atoms were stable during calcination in air, even at high temperatures (Extended Data Fig. 4e-f)[8,12]. During H_2 reduction at 300 °C for 1 h, however, the CeO_2-supported Pt atoms sintered to form Pt NPs (Extended Data Fig. 7a-c), implying that the Pt-O-Ce bonds were broken and the Pt atoms moved on reducible CeO_2 surfaces. After H_2 reduction treatment, the sizes of Pt particles on CeO_2 powders were smaller than those on SiO_2 (Extended Data Fig. 7a-b and 6c-d), confirming that the Pt-CeO_2 interaction is much stronger than the Pt-SiO_2 interaction under an H_2 atmosphere. Dispersed Pt atoms on CeO_2 surfaces, however, became mobile at temperatures ≥ 300°C under H_2 environment. In stark contrast, the Pt atoms in the 0.4 wt% $Pt/CeO_{1.86}/SiO_2$ catalyst did not show any sign of sintering, even after H_2 reduction treatment at 300 °C for 10 h, as evidenced by DRIFTS spectra and HAADF-STEM images (Fig. 3d and Extended Data Fig. 8a-b). To further probe the stability of Pt atoms localized on the $CeO_{1.86}$ nanoglue islands, catalyst samples were exposed to H_2 at 400 °C to 600 °C. Even under such harsh reduction conditions, the Pt atoms remained cationic (Extended Data Fig. 8c-e). For catalysts that were reduced above 500 °C, however, significantly blue-shifted CO absorption peaks were observed, probably suggesting a major modification of the Pt-$CeO_{1.86}$ interaction. Although we could not rule out the possibility that Pt atoms moved within their own $CeO_{1.86}$ nanoglue islands during H_2 treatment but the Pt atoms did not move onto the SiO_2 surfaces—if they had, Pt clusters and particles would have been readily detected by HAADF-STEM imaging and DRIFTS.

Taking these results together, we infer that both the SiO_2-supported $CeO_{1.86}$ nanoglue islands and CeO_2 NPs confine movement of Pt atoms during the H_2 reduction treatment and that Pt clusters should form if each $CeO_{1.86}$ nanocluster or CeO_2 NP contains more than one Pt atom. To further test the hypothesis that Pt atoms on CeO_2 sinter under H_2 reduction treatment, a catalyst which contained Pt atoms dispersed on CeO_2 NPs, denoted as 0.4 wt% Pt/CeO_2 NPs/SiO_2 SAC, was exposed to H_2 at 300 °C for 1 h. All the experimental characterization data (Extended Data Fig. 7d-i) show that although the Pt atoms did not migrate onto the SiO_2 surfaces to form larger particles they did sinter to form small Pt clusters on the CeO_2 NPs—because some of the larger CeO_2 NPs evidently contained more than one Pt atom. The CO DRIFTS spectra (Extended Data Fig. 7g-h) clearly show the representative peaks of CO adsorbed on Pt clusters/NPs. Because of the lower Pt loading (0.4 wt%), some CeO_2 particles might still contain single Pt atoms after the reduction treatment. In striking contrast to the relatively sharp DRIFTS peak on the 0.4 wt% Pt/$CeO_{1.86}$/SiO_2 (Fig. 3d), the broad overlapping DRIFTS peaks on the reduced 0.4 wt% Pt/CeO_2 NPs/SiO_2 SAC clearly demonstrate the presence of highly heterogeneous dispersity of the Pt species on the CeO_2 NPs.

To further verify our conclusion that during a high-temperature H_2 reduction process, Pt atoms located on the same $CeO_{1.86}$ cluster sinter while Pt atoms located on different $CeO_{1.86}$ clusters do not move together to sinter, high amount of Pt (4 wt%) atoms were loaded onto SiO_2 supported $CeO_{1.86}$ clusters to produce a Pt cluster catalyst. After reducing the 4 wt% Pt/$CeO_{1.86}$/SiO_2 catalyst in H_2 at 300 °C for 3 h, Pt clusters/NPs were clearly detected by CO DRIFTS (Extended Data Fig. 8f). Uniform Pt clusters, with an average size of ~0.9 nm when the reduction temperature was increased to 400 °C, were attached onto the $CeO_{1.86}$ nanoglue islands (Extended Data Fig. 8g). After a more severe reduction, at 500 °C for 12 h, the $CeO_{1.86}$ nanoglue islands became amorphous; the Pt clusters, however, retained their sizes and were still attached to the $CeO_{1.86}$ nanoglue islands, unambiguously indicating strong adhesion between Pt species and the $CeO_{1.86}$ nanoglue islands (Extended Data Fig. 8h). The absence of Pt particles with sizes >1 nm in diameter in these highly reduced catalysts is a clear manifestation of localization of the Pt species onto the $CeO_{1.86}$ nanoglue islands even when the Pt species become mobile on their own $CeO_{1.86}$ nanoglue islands—no cross-movement of Pt species among the CeO_x nanoclusters. These results firmly demonstrate that our localization design applies not only to supported metal atoms but also supported subnanometer metal clusters (Extended Data Fig. 8i), significantly expand practical applications of our nanoglue localization strategy in contrast to previous stabilization approaches[24,28-30].

For many catalytic reactions, the active phase is usually activated by H_2 reduction prior to a desired catalytic reaction. For metal-oxide-supported SACs, H_2 treatment at temperatures > 200 °C usually causes sintering of metal atoms[12,13]. Because of such detrimental sintering effects, many SACs were directly used without being activated by such a H_2 reduction treatment, hindering the true measurement of the catalytic performance of the as-prepared SACs. Due to saturation by oxygen ligands, many SACs may not show catalytic activity after a moderate- to high-temperature calcination treatment. Since our 0.4 wt%

$Pt/CeO_{1.86}/SiO_2$ SACs resist sintering during H_2 activation processes, we can quantitatively evaluate how the H_2 activation process affects CO oxidation on $CeO_{1.86}$ nanoglue supported Pt_1 atoms. Prior to the H_2 reduction treatment, the as-synthesized 0.4 wt% $Pt/CeO_{1.86}/SiO_2$ SAC had relatively low activity for CO oxidation (Fig. 4), in agreement with reports on Pt_1/CeO_2 SACs[8,12-13]. The H_2 activated $Pt/CeO_{1.86}/SiO_2$ SAC, however, achieved 50% and 90% CO conversion at 133 °C and 142 °C, respectively. For comparison, the T_{50} (temperatures for 50% CO conversion) for the activated $Pt/CeO_{1.86}/SiO_2$ (impregnation-IMP)) and activated Pt/SiO_2 (IMP) catalysts were 171 and 227 °C (Fig. 4b), respectively. In particular, the H_2 activation process had a much bigger effect on impregnated Pt species supported on reducible $CeO_{1.86}$ nanoclusters than on Pt species supported on nonreducible SiO_2, because $Pt/CeO_{1.86}/SiO_2$ (IMP) showed higher activity and Pt dispersion than Pt/SiO_2 (IMP) after H_2 reduction (Extended Data Fig. 9a-d).

The turn-over-frequency (TOF) and specific reaction rate (normalized by Pt mass) under similar CO oxidation conditions were evaluated for the various catalysts (Extended Data Fig. 9e). The TOF for CO oxidation on the as-synthesized 0.4 wt% $Pt/CeO_{1.86}/SiO_2$ SAC was 0.012 s^{-1} at 150 °C, similar to the reported value[13]. The H_2 activation markedly increased the TOF to 1.8 s^{-1}, 150 times higher than that of the non-activated catalyst. The specific rate at 150 °C on the activated 0.4 wt% $Pt/CeO_{1.86}/SiO_2$ SAC was 20 and 204 times higher than that on the activated 0.4 wt% $Pt/CeO_{1.86}/SiO_2$ (IMP) and Pt/SiO_2 (IMP), respectively. The activated 0.4 wt% $Pt/CeO_{1.86}/SiO_2$ SAC possesses the lowest apparent activation energy (E_a = ~68 kJ/mol) (Extended Data Fig. 9f) and was stable during four separate light-off cycles (Fig. 4a). Time-on-stream conversion test at 140 °C verified the long-term stability of the activated 0.4 wt% $Pt/CeO_{1.86}/SiO_2$ SAC (Extended Data Fig. 9g-h).

In summary, we developed a scalable and practical process to localize Pt atoms on functional CeO_x (x = 1.86 by XPS measurement) nanoglue islands (average size = ~ 2nm) dispersed on a robust, high-surface-area SiO_2 support. A facile and scalable SEA process was used to synthesize both the ultra-small, isolated $CeO_{1.86}$ nanoglue islands and the selective deposition of Pt atoms onto only those $CeO_{1.86}$ nanoglue islands. The SiO_2-supported $CeO_{1.86}$ nanoglue islands possess abundant Ce^{3+} species, and strongly anchor and localize Pt atoms/clusters under both O_2 or H_2 environment, even at elevated temperatures. For CO oxidation reaction, activation of $CeO_{1.86}$-supported Pt atoms increased the TOF by 150 times. The CeO_x nanoglue islands not only localize Pt atoms to prevent sintering but also provide facile oxygen during CO oxidation reaction. Our strategy to confine the movement of metal atoms by isolated nanoglue islands extends to metals other than Pt (Extended Data Fig. 10). The use of functional nanoglues on robust high-surface-area supports to localize metal atoms can be broadly applied to creating a wide range of robust single-atom catalysts for a plethora of important catalytic transformations.

Declarations

Data availability. The data that support the findings of this study are available from the corresponding author upon reasonable request.

Acknowledgements

This work was supported by the National Science Foundation under Grant No. 1465057 (CHE-1465057) and 1955474 (CHE-1955474). X.I.P.-H. and Y.W. acknowledge the support by U.S. Department of Energy (DOE), Basic Energy Sciences (SC), Division of Chemical Sciences (DE-FG02-05ER15712). C.-Y.F. and BCG acknowledge the support of DOE SC grant DE-FG02-04ER15513. X.I.P.-H. also thanks Fulbright Colombia and Colciencias for part of the financial support provided to pursue a Ph.D. X.L. acknowledges funding from the China Scholarship Council (CSC) (201706340130).

Author contributions

J.L. conceived the concept and designed the studies. X.L. designed the synthesis methods, conducted all synthesis work and catalytic tests, and conducted some of the DRIFTS experiments. X.I.P.-H. and Y.W. carried out CO DRIFTS experiments during the early stages of this project. C.F., Y.C. and B.G. performed experiments and analyzed XANES and EXAFS data. J.L. conducted the STEM imaging and analyses. J.Z. provided suggestions on the research project. X.L. and J.L. wrote the manuscript. All authors discussed the results and commented on the manuscript.

Competing financial interests

The authors declare no competing financial interests.

Additional information

Supplementary information is available in the online version of the paper. Reprints and permissions information is available online at www.nature.com/reprints.

Correspondence and requests for materials should be addressed to J.L.

References

1. Qiao, B. *et al.* Single-atom catalysis of CO oxidation using Pt_1/FeO_x. *Nat. Chem.* **3**, 634 (2011).
2. Liu, L. & Corma, A. Metal catalysts for heterogeneous catalysis: from single atoms to nanoclusters and nanoparticles. *Chem. Rev.* **118**, 4981-5079 (2018).
3. Wang, A., Li, J. & Zhang, T. Heterogeneous single-atom catalysis. *Nat. Rev. Chem.* **2**, 65-81 (2018).
4. Gates, B. C. Atomically dispersed supported metal catalysts: Seeing is believing. *Trends in Chemistry* **1**, 99-110 (2019).

5. Li, Z., *et al.* Well-defined materials for heterogeneous catalysis: From nanoparticles to isolated single-atom sites. *Chem. Rev.* **120**, 623-682 (2020).
6. Hülsey, M. J., Zhang, J. & Yan, N. Harnessing the wisdom in colloidal chemistry to make stable single-atom catalysts. *Adv. Mater.* **30**, 1802304 (2018).
7. Qin, R., Liu, P., Fu, G. & Zheng, N. Strategies for stabilizing atomically dispersed metal catalysts. *Small Methods* **2**, 1700286 (2018).
8. Jones, J. *et al.* Thermally stable single-atom platinum-on-ceria catalysts via atom trapping. *Science* **353**, 150-154 (2016).
9. DeRita, L. *et al.* Structural evolution of atomically dispersed Pt catalysts dictates reactivity. *Nat. Mater.*, **18**, 746-751 (2019).
10. Ren, Y. *et al.* Unraveling the coordination structure-performance relationship in Pt_1/Fe_2O_3 single-atom catalyst. *Nat. Commun.* **10**, 4500 (2019).
11. Duan, S., Wang, R. & Liu, J. Stability investigation of a high number density Pt_1/Fe_2O_3 single-atom catalyst under different gas environments by HAADF-STEM. *Nanotechnology* **29**, 204002 (2018).
12. Pereira-Hernández, X. I. *et al.* Tuning Pt-CeO_2 interactions by high-temperature vapor-phase synthesis for improved reducibility of lattice oxygen. *Nat. Commun.* **10**, 1358 (2019).
13. Wang, H. *et al.* Surpassing the single-atom catalytic activity limit through paired Pt-O-Pt ensemble built from isolated Pt_1 atoms. *Nat. Commun.* **10**, 3808 (2019).
14. Liang, J. *et al.* Heterogeneous Catalysis in Zeolites, Mesoporous Silica, and Metal-Organic Frameworks. *Adv. Mater.* **29**, 1701139 (2017).
15. Bruix, A. *et al.* Maximum noble-metal efficiency in catalytic materials: atomically dispersed surface platinum. *Angew. Chem. Int. Ed.* **53**, 10525-10530 (2014).
16. Wan, J. *et al.* Defect effects on TiO_2 nanosheets: stabilizing single atomic site Au and promoting catalytic properties. *Adv. Mater.* **30**, 1705369 (2018).
17. Lang, R. *et al.* Non defect-stabilized thermally stable single-atom catalyst. *Nat. Commun.* **10**, 234 (2019).
18. Li, J. *et al.* Highly active and stable metal single-atom catalysts achieved by strong electronic metal-support interactions. *J. Am. Chem. Soc.* **141**, 14515-14519 (2019).
19. Vayssilov, G. *et al.* Support nanostructure boosts oxygen transfer to catalytically active platinum nanoparticles. *Nat. Mater.* **10**, 310-315 (2011).
20. Lykhach, Y. *et al.* Counting electrons on supported nanoparticles. *Nat. Mater.* **15**, 284-288 (2016).
21. Wong, A., Liu, Q., Griffin, S., Nicholls, A. & Regalbuto, J. Synthesis of ultrasmall, homogeneously alloyed, bimetallic nanoparticles on silica supports. *Science* **358**, 1427-1430 (2017).
22. Wu, Z. *et al.* Probing Defect Sites on CeO_2 Nanocrystals with Well-Defined Surface Planes by Raman Spectroscopy and O_2 Adsorption. *Langmuir* **26**, 16595-46606 (2010).

23. Kato, S. *et al.* Quantitative depth profiling of Ce^{3+} in Pt/CeO_2 by in situ high-energy XPS in a hydrogen atmosphere. *Phys. Chem. Chem. Phys.* **17**, 5078-5083 (2015).
24. Jeong, H. *et al.* Controlling the Oxidation State of Pt Single Atoms for Maximizing Catalytic Activity. *Angew. Chem. Int. Ed.* **59**, 20691-20696 (2020).
25. De Faria, L. A. & Trasatti, S. The point of zero charge of CeO_2. *J. Colloid Interface Sci.* **167**, 352-357 (1994).
26. Liu, J. Aberration-corrected scanning transmission electron microscopy in single-atom catalysis: Probing the catalytically active centers. *Chinese J. Catal.* **38**, 1460-1472 (2017).
27. Kottwitz, M. *et al.* Local structure and electronic state of atomically dispersed Pt supported on nanosized CeO_2. *ACS Catal.* **9**, 8738-8748 (2019).
28. DeRita, L. *et al.* Catalyst Architecture for Stable Single Atom Dispersion Enables Site-Specific Spectroscopic and Reactivity Measurements of CO Adsorbed to Pt Atoms, Oxidized Pt Clusters, and Metallic Pt Clusters on TiO_2. *J. Am. Chem. Soc.* **139**, 14150-14165 (2017).
29. Ma, G. *et al.* Stabilizing gold clusters by heterostructured transition-metal oxide-mesoporous silica supports for enhanced catalytic activities for CO oxidation. *Chem. Commun.* **48**, 11413-11415 (2012).
30. Alexeev, O., Shelef, M. & Gates, B. C. MgO-Supported Platinum-Tungsten Catalysts Prepared from Organometallic Precursors: Platinum Clusters Isolated on Dispersed Tungsten. *J. Catal.* 164, 1 (1996).

Figures

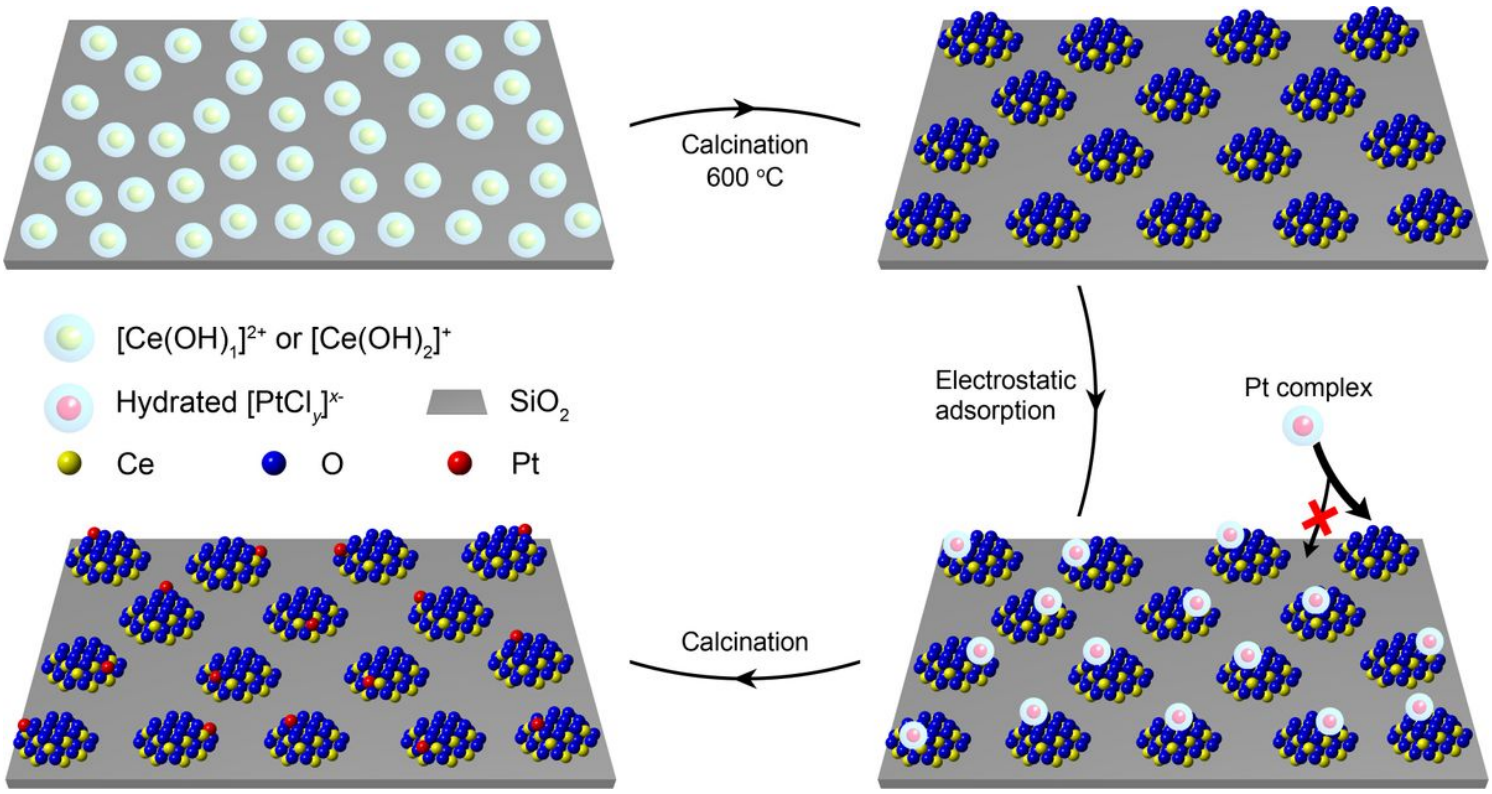

Figure 1

Schematic diagrams illustrate the fabrication processes of CeOx/SiO2 supported Pt1 SACs. The [Ce(OH)2]+ and [Ce(OH)]2+ precursor species are produced in situ from Ce3+ reacting with OH- species in a mild alkaline solution. The positively charged Ce-containing species electrostatically adsorb onto negatively charged surfaces of the high-surface-area SiO2 support. After high-temperature calcination, atomically dispersed Ce species self-assemble into crystalline CeOx nanoclusters. These ultra-small CeOx nanoclusters act as functional nanoglues to localize metal atoms and to provide surface active oxygen species. By judiciously adjusting the aqueous solution to 6≥pH≥4 where CeOx nanoclusters are positively charged and SiO2 surfaces are negatively charged, the negatively charged Pt-containing species adsorb only onto the CeOx nanoclusters. Subsequent rigorous washing and high-temperature calcination processes eliminate solution residues and facilitate confinement of Pt atoms to only the crystalline CeOx nanoclusters.

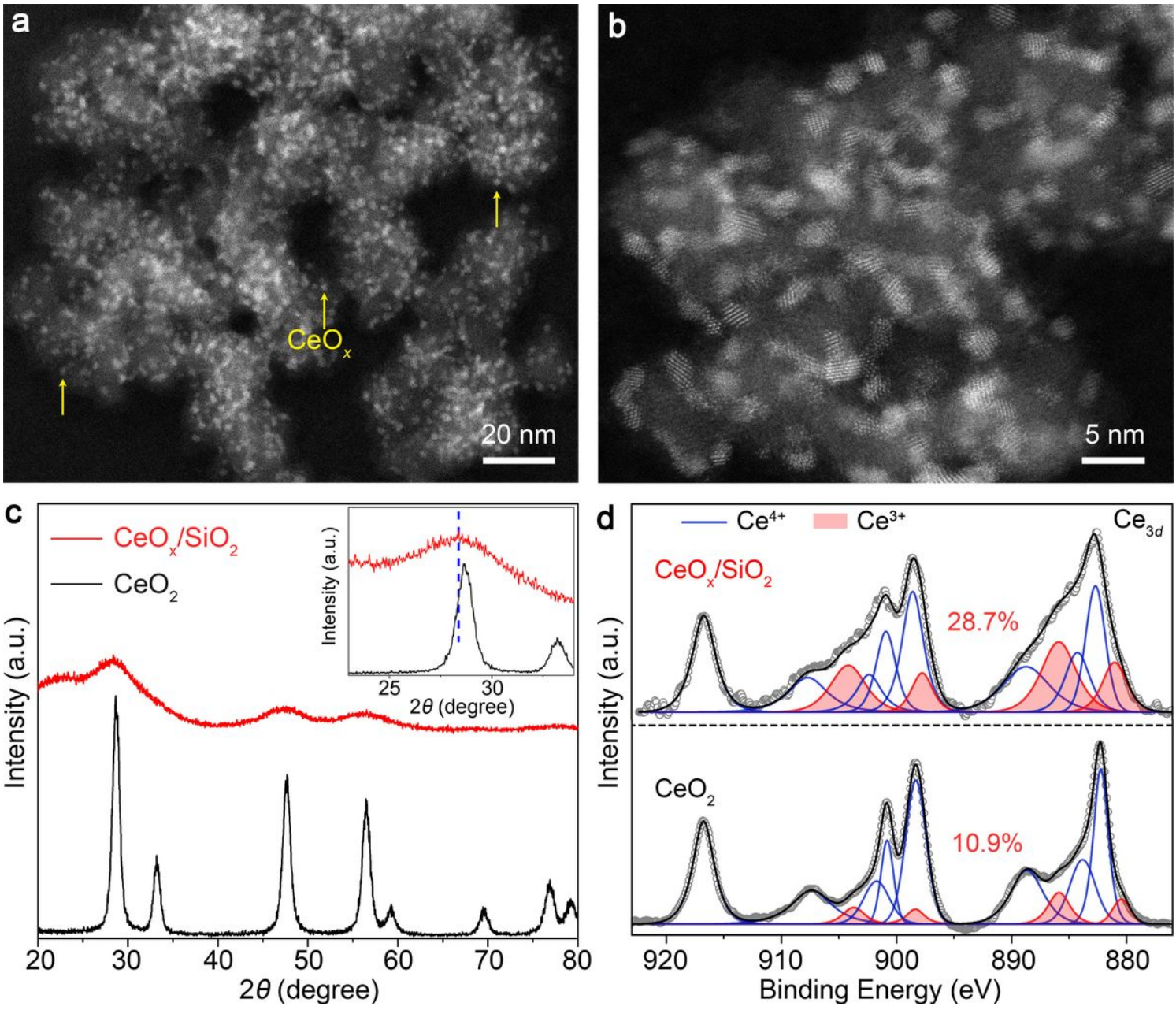

Figure 2

Electron microscopy, X-ray diffraction and XPS characterization of CeOx nanoglue islands dispersed onto high-surface-area SiO2. a, Low magnification HAADF-STEM image of the as-prepared CeOx nanoclusters conformally coating the high-surface-area SiO2 support. b, Atomic-resolution HAADF-STEM image of crystalline CeOx nanoclusters. c, Powder XRD patterns of pure CeO2 NPs and CeOx/SiO2 (arbitrary units). The inset shows broadening and red-shift of peak position from CeOx nanoclusters. d, Ce 3d XPS spectra obtained from SiO2 supported CeOx nanoclusters (top panel) and pure CeO2 powders (bottom panel). The CeOx nanoclusters clearly contain much higher amount of oxygen vacancies (represented by the higher % of Ce3+) than those of the well-crystallized CeO2.

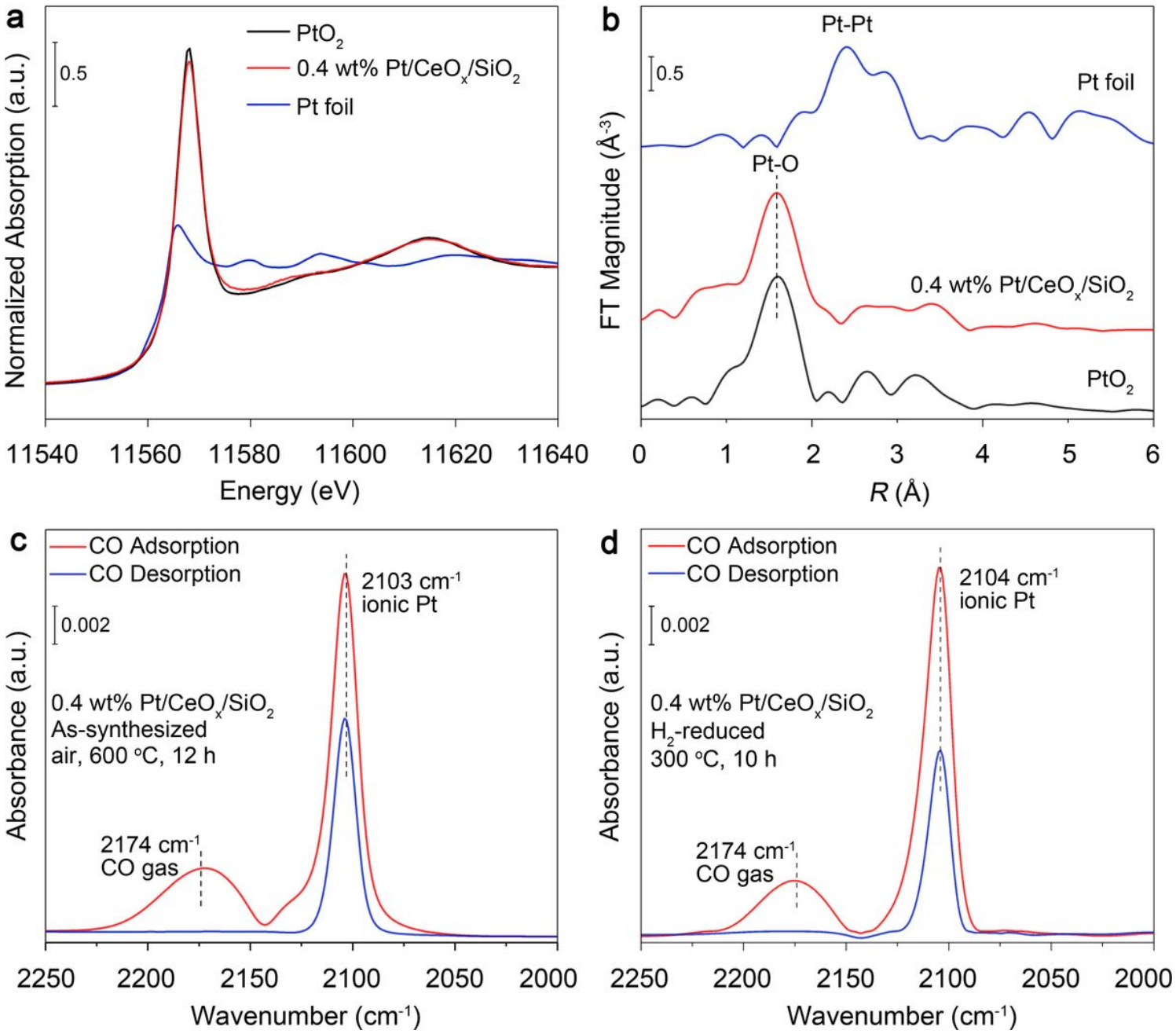

Figure 3

Identification of Pt atoms on CeO1.86 nanoglue islands. a, Pt LIII XANES spectrum obtained from the 0.4 wt% Pt/CeO1.86/SiO2 catalyst. b, the corresponding Fourier transform radial distribution function of Pt LIII-edge k3-weighted EXAFS spectrum. The XANES and EXAFS spectra from Pt foil and bulk PtO2 were obtained as references. c, CO adsorption DRIFTS on the as-synthesized 0.4 wt% Pt/CeO1.86/SiO2 catalyst which was oxidized in air at 600 °C for 12 h. After 20 min of CO adsorption (red line), the CO flow was discontinued, and the CO desorption spectrum was recorded at a steady state after purging with He (blue line); sample temperature: 100 °C. d, CO adsorption and desorption DRIFTS on the reduced (H2 at 300 °C for 10 h) 0.4 wt% Pt/CeO1.86/SiO2 catalyst. Both the calcined and reduced 0.4 wt% Pt/CeO1.86/SiO2 catalyst contained only single Pt atoms.

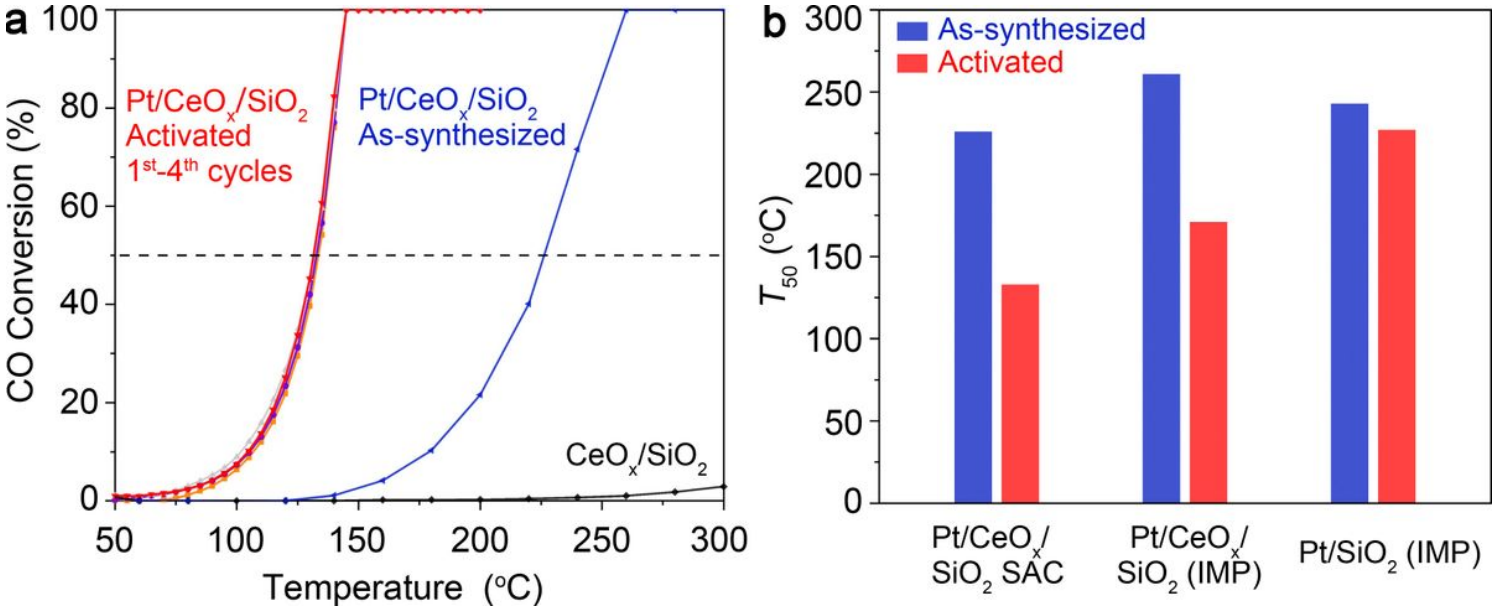

Figure 4

Evaluation of CO oxidation activity and stability. a, CO conversion versus reaction temperature over the as-synthesized and activated 0.4 wt% Pt/CeO1.86/SiO2 SAC (CO oxidation on the CeO1.86/SiO2 control catalyst is also shown). b, Light-off temperatures (T50) of different catalysts with the same amount of Pt loading: Pt/CeO1.86/SiO2 SAC, Pt/CeO1.86/SiO2 (IMP) and Pt/SiO2 (IMP). Activation of the 0.4 wt% Pt/CeO1.86/SiO2 SAC significantly increased activity for CO oxidation and the activated 0.4 wt% Pt/CeO1.86/SiO2 SAC was stable during CO oxidation reaction.

Supplementary Files

This is a list of supplementary files associated with this preprint. Click to download.

- NanoglueSupportedSingleAtomCatalystsSIJLiuofASU.doc